pH-Dependent Nanodiamonds Enhance the Mechanical Properties of 3D-Printed Hyaluronic Acid Nanocomposite Hydrogels

Dae Gon Lim
Dongguk University
Eunah Kang (eakangek@cau.ac.kr)
Chung-Ang University
Seong Hoon Jeong
Dongguk University

Research

Keywords: nanocomposite hydrogel, nanodiamond, surface modification, compressive stress, mechanical property

Posted Date: June 10th, 2020

DOI: https://doi.org/10.21203/rs.3.rs-18085/v2

Version of Record: A version of this preprint was published at Journal of Nanobiotechnology on June 10th, 2020. See the published version at https://doi.org/10.1186/s12951-020-00647-w.

Abstract

Nanocomposite hydrogels capable of undergoing manufacturing process have recently attracted attention in biomedical applications due to their desired mechanical properties and high functionality. 3D printing nanocomposite hydrogels of hyaluronic acid (HA)/nanodiamond (ND) revealed that the addition of ND with the low weight ratio of 0.02 wt % resulted in higher compressive force and gel breaking point, compared with HA only nanocomposites. These HA nanocomposite hydrogels loaded with surface functionalized ND allowed for the enforced compressive stress to be tuned in a pH-dependent manner. HA nanocomposite hydrogels with ND-OH at pH 8 showed an increase of 1.40 fold (0.02%: 236.18 kPa) and 1.37 fold (0.04%: 616.72 kPa) the compressive stress at the composition of 0.02 wt % and 0.04 wt, respectively, compared to those of ND-COOH (0.02%: 168.31 kPa, 0.04%: 449.59 kPa) at the same pH. Moreover, the compressive stress of HA/ND-OH (0.04 wt %) at pH 8 was mechanically enhanced 1.29 fold, compared to that of HA/ND-OH (0.04 wt %) at pH 7. These results indicate that the tunable buffering environment and interaction with the long chains of HA at the molecular level have a critical role in the dependency of the mechanical properties on pH. Due to the pH stability of the ND-OH nanophase, filament-based processing and layer-based deposition at microscale attained enforced mechanical properties of hydrogel. Fine surface tuning of the inorganic ND nanophase and controlled 3D printing leads to improved control over the pH-dependent mechanical properties of the nanocomposite hydrogels reported herein.

Introduction

Three-dimensional (3D) printing of biomaterials has gained attention in the pharmaceutics to direct development toward customized therapeutics that increase patient compliance. Computation-based manufacturing processes, including tablets [1], medical devices [2, 3], tissue engineering [4-6], and tumor modeling [7] have benefited from 3D printing. Layer-by-layer-based construction provides exquisite control over parameters such as drug amount, size, multidrug loading, scaffold porosity, and release profiles simply through geometric modification. 3D printing can be classified into several categories including stereolithographic printing by UV irradiation, powder bed/powder jetting system, selective laser sintering of thermoplastic polymer, and extrusion-based system [1, 3]. Processing ink materials has a pivotal role in the choice of mechanical 3D-printing type; the geometric shape and stability of the constructed filaments from the nozzle depend on the ink’s physical and chemical properties, including thermoplasticity, UV curability, and rheological properties.

The functionality of a thermoplastic biodegradable polymer or natural biopolymer with versatile chemical modification has been extensively studied for theranostics and drug delivery. There have been several recent studies exploring the microscopic mechanical properties of these polymers, as well as their cellular functionality and drug delivery [8-13]. In particular, modified nanocomposite hydrogels with enhanced mechanical and functional properties have been beneficial in the fields of tissue engineering, medical devices, and depot formulation. Scalable micro-environments created by 3D printing have allowed for the study of cell proliferation and estimated tumor modeling of breast cancer bone metastasis, with relation

to geometric factors [7]. Even the distribution of metallic ions in 3D hydrogel has been shown to amplify the signal intensity of DNA sensing [14]. Mechanically enhanced biomaterials and natural biopolymers have been composited with metal [15], carbon based materials [15-19], glass [20-22], cellulose crystal [23, 24], and clay [25, 26] to form nanocomposites for a variety of applications. Nanocomposite hydrogels that incorporate diverse nanophase inorganic particles are challenging because metastatic materials mimicking biological tissues require a variety of considerations including softness, biocompatibility, strength, and structurally compatible elasticity. The specific functionality granted by nanocomposite hydrogels with inorganic materials would lead to improved electrical conductivity [27, 28], energy absorbance [29-31], as well as cellular [18, 26, 32, 33] and protein interactions [2], in addition to mechanical enhancement.

Hyaluronic acid (HA), is a natural non-immunogenic biopolymer that is ubiquitous in connective tissue. HA has been used for various forms of medicine and long-term release implant in vivo. HA has the advantage that data on safety in the human body are present in large quantities compared to other artificial polymers. In addition, HA is easy to perform chemical modification, which can modify the physicochemical properties [34]. Due to the above advantages, various studies on chemically modifying HA as bioink for 3d printing have been conducted such as pentenoate-functionalized HA [35], β-cyclodextrin /adamantane induced HA [36, 37]. In this study, commonly used crosslinkable methacrylated HA was used for nanocomposite hydrogel with addition of nanodiamonds for 3D processable printing.

Among the nanoscale carbon based materials, nanodiamonds (NDs) have been chosen due to their hydrophilicity and pH-dependent surface functionality, along with their convenient chemical modality.[38-40] Detonated NDs, of approximately 5 nm, followed by an acid-wash are amenable to a diverse range of surface modifications. Depending on the tunable surface properties, NDs can be created as agglomerates ranged from approximately 5 nm to several hundred nm in size [41]. These 5 nm NDs have been used to deliver small hydrophobic chemical drugs [42] and negatively charged RNA [43], as well as crosslinked for thermoplastic composites [39]. The high surface-to-volume ratio and inert hardness also provided lubrication to reduce friction and wear for even biomaterials, which is an important parameter in the extrusion-based 3D-printing process [44]. Here, nanocomposite hydrogels mixed with UV-crosslinkable HA and surface-modified NDs were processed using a nozzle-based extrusion 3D-printing manufacturing system (Scheme 1b). The rheological properties of nanocomposite hydrogel precursor and mechanically enforced nanocomposite hydrogels were characterized with the addition of carboxylated and hydroxylated NDs at varied pH.

Experimental Methods

Due to technological limitations, the Experimental Methods section is only available as a download in the supplementary files section.

Results And Discussion

The rheological properties of hydrogel precursor of HA/ND were determined with viscosity change and shear rate. To prepare nanocomposite hydrogel precursors, 0.02 wt % carboxylated or hydroxyl ND were mixed with 2 wt % of MeHA at pH 7 and pH 8. After the full pre-sheared state of the nanocomposite hydrogel precursor, the shear rate decreased significantly and the viscosity change is recorded during the subsequent 100 sec. As shown in Figure 1, the shear-thinning effect of all HA, HA/ND-COOH, and HA/ND-OH nanocomposite hydrogel precursor generated low viscosities (approximately 2 Pa·s) in the pre-sheared zone. After the shear rate was decreased and fluids were fully structured, the viscosity of the nanocomposite hydrogel precursors increased rapidly with a stiff gradient to approximately 33.24 Pa·s on average in 2/s. The viscosity of the nanocomposite hydrogel precursors with nanodiamonds was 35.74 Pa·s for ND-COOH and 27.5 Pa·s for ND-OH at pH 7, respectively. In addition, the viscosity of MeHA was 13.34 Pa·s at pH 7 and 32.29 Pa·s in 2/s. It is noted that nanocomposite HA hydrogel containing NDs showed higher viscosity and shorter response time, compared to HA only hydrogels, indicating a pH controllable filament shape in the 3D-printing process. The nanocomposite HA hydrogel precursors showed higher viscosity at pH 8, compared to those at pH 7. Rheological characteristics such as viscosity may vary depending on the degree of polymerization of HA, but by using ND, it was possible to form a viscosity suitable for printing despite the use of a lower content of HA. Compared to the results obtained by measuring the viscosity using a commercially available product (Cellink®) and pentenoate-functionalized HA, viscosity in 2/s was 52.8 Pa·s for HA/ND-COOH (at pH 8), about 100 Pa·s for Cellink®, and 120 Pa·s for 3% pentanoate functionalized HA [35]. Compared to the results of other studies, the viscosity was relatively low, but concentration of hyaluronic acid (2 wt %) was lower than other hydrogel (at least 3%), and HA/ND hydrogel showed stronger shear thinning effect than other materials. As the nanodiamond was added, the increased viscosity increased up to 270% compared to when HA was used alone, but it was confirmed that the viscosity decreased very rapidly with increasing shear rate. HA/ND-COOH (at pH 8) showed the highest viscosity 15.33 Pa at 10/s, which is a 70% decreased value from initial viscosity. Weak shear-thinning originates from high molecular weight hyaluronic acid itself [48], but nanodiamonds appear to induce shear-thinning more strongly. Shear-thinning hydrogels were researched by blending shear-thinning materials to hyaluronic acid [13, 36] and nanodiamonds performed a similar role in hyaluronic acid. As the negatively charged end groups of HA and ND increased, electrostatic interaction between nanophase ND and HA resulted in the augmented viscosity, which was further influenced by the 3D-printing manufacturing process.

The change of zeta potential and hydrodynamic diameter of ND-OH and ND-COOH agglutinates depending on pH were fully characterized in previous study [42]. In brief, the zeta potentials of ND–COOH were negative −22.5 ± 0.2 mV and −27.0 ± 0.4 mV, at pH 7 and pH 8, respectively. ND–COOH dispersion showed the decrease in zeta potential as the increased pH from 7 to 8 due to deprotonation of carboxyl groups. ND–OH produced by the reduction of ND–COOH showed stable zeta potentials in the wide pH ranges, ranged from −51.4 ± 0.9 mV to −44.5 ± 0.7 mV at the pH 4 - 10. The zeta potentials of ND–COOH and ND–OH were negative zeta potential of −22.5 ± 0.2 mV and −42.7 ± 1.2 mV at pH 7, respectively, suggesting good colloidal stability. The diameters of the dispersed ND–OH and ND–COOH agglutinate were also affected by environmental pH. Depending on the pH, the average sizes of ND–COOH were

changed into 105.2 nm at pH 7 and 77.9 ± 1.6 nm at pH 8. The average sizes of ND–OH were 61.5 ± 0.3 nm at pH 7 to 67.2 ± 3.3 nm at pH 8, showing less pH sensitivity and high dispersion stability. These pH dependence by surface functional group. pH dependent size changes of ND agglutinates are closely related with the dissociation constants (pKa) of carboxylic acids 5.0 and the alcohol 14–16, as reported. The degree of ionization might determine colloidal stability and resulting agglutinate size due to interparticle interaction.

Regarding with these, pH dependent colloidal stability and negative zeta potentials of ND-COOH and ND-OH might have repulsive electrostatic interaction between negative HA. The agglutinate size resulted from environmental pH dependent charge effect might also contribute the significantly increased shear thinning effect. Considering that size of ND-COOH became significantly increased at pH 7, increased shear thinning effect should be considered with colloidal size. ND-OH with smaller stabilized particle size and higher negative zeta potentials showed less shear thinning effect, compared to the ND-COOH. Resulting shear thinning effect by addition of NDs might be complex of factors including colloidal size, surface charge, surface functionality. The resulting higher shear thinning effect by addition of ND, compared to HA only gained the processible high quality of printing ink.

Shear thinning was observed using nanocomposite hydrogel precursors, which can be attributed to the electrostatic interactions from the COO- and hydrogen bonding (-OH) between ND surface and HA. The rheological properties of the nanocomposite hydrogel precursors estimated as storage modulus G' and loss modulus G" revealed that the HA/ND-COOH and HA/ND-OH hydrogel increased by 1.18 (185.4 Pa) and 1.13 (177.6 Pa) fold (G'), 1.10 (67.86Pa) and 1.02 (63.24 Pa) fold (G") at pH 7, respectively, compared to HA only hydrogel at 62.83 rad/s (10 Hz) (Figure 2a). This result suggests that the existence of physical interaction, i.e., electrostatic interaction between –COO– on the ND surface and HA chains, contributes to the increase in G' and G" in HA/ND hydrogel precursors. Remarkably, G' and G" in HA/ND-COOH hydrogel precursor at pH 8 was increased 1.4 fold (260.5 Pa) and 1.26 fold (85.26 Pa), respectively, compared with those of HA/ND-COOH hydrogel at pH 7. This proves that the deprotonated ND-COOH surface became hydrophilic and was interacting with the HA chains. In a pH dependent manner, the shear-thinning behavior of the HA/ND hydrogels precursor occurred through quick absorption and desorption of HA chains from ND surface, affecting the 3D printing structure and filament stability.

The filament diameter is generally controlled by operating parameters including the inner diameter of the needle, nozzle path speed, and standoff distance on the filament width. When deposited as a liquid filament of nanocomposite hydrogel precursor, filament structure and stability are critical during the extrusion. In general, filament widths can be controlled by varying the pressure of the cylinder, the inner diameter of the nozzle, the path speed, and the standoff distances [11, 49]. A 26 gauge needle was used to extrude stable filaments of the HA/ND-COOH and HA/ND-OH hydrogel nanocomposites, demonstrated in Figure 3. The same operating conditions were used to explore the dependence of mechanical properties on pH between the different NDs.

The 3D-printed nanocomposite hydrogels with spatiotemporal 3D printing construction were visualized both optically and with SEM. The HA nanocomposite hydrogel revealed that the 3D-dimensional porous networked structure was uniformly distributed with an average pore size of 128 μm (Figure 4a and 4b). Reproducibility in size, shape, and fidelity of structure are shown as optical images in Figure 4c and 4d.

The compressive mechanical stress of nanocomposite hydrogels containing ND-COOH and ND-OH were compared with HA only hydrogels. Nanocomposite hydrogel precursors of HA/ND-COOH and HA/ND-OH were prepared using either 0.02 wt % or 0.04 wt % ND with 2 wt % of MeHA and printed using predetermined printing conditions. The highest level of compressive stress was observed in the vicinity of 90-93% of the compressive strain, and a gel breakage was observed when strain was higher than 90% of the strain. The 3D structure of HA/ND-COOH (0.02 wt %) and HA/ND-OH(0.02 wt %) nanocomposite hydrogels showed maximum compressive stresses of 152.82 kPa, and 161.59 kPa at pH 7, showing 2.2 fold and 2.35 fold, respectively, higher than the HA only hydrogels (68.72 kPa) (Figure 5a). With the addition of higher composition of ND-COOH (0.04 wt %), the compressive stress was increased by 163 %, compared to that of the lower composition ND-COOH hydrogel (0.02 wt %). Moreover, the 0.04 wt % composite ratio of ND-OH resulted in the stiffest gradient and dramatically enhanced peak compressive force of 296% (478.03 kPa), compared to that of hydrogel for ND-COOH (0.02 wt %). Similar compressive stress was observed for HA/ND-COOH and HA/ND-OH nanocomposite hydrogels when processed at pH 8 (Figure 5b). HA nanocomposite hydrogels with ND-OH at pH 8 showed an increase of 1.40 fold (236.18 kPa) and 1.37 fold (616.72 kPa) compressive stress at the composition of 0.02 wt % and 0.04 wt %, respectively, compared to those of ND-COOH (168.31 kPa (0.02wt% ND-COOH), 449.59 kPa(0.04 wt% ND-COOH)) at the same pH 8. Moreover, the compressive stress of HA/ND-OH (0.04 wt %) at pH 8 was mechanically enhanced 1.29 fold, compared to that of HA/ND-OH (0.04 wt %) at pH 7.

The results indicate that 3D printed HA hydrogels filled with hydrophilic surface functionalized nanodiamond boost mechanical properties even at low weight ratios of ND. The enhanced mechanical properties can be attributed to the high surface-to-volume ratio and hydrophilic ND surface which generated sufficient nanophase distribution within hydrogel matrix [50].

The comparison of pH dependence and the effect of surface functional groups are also apparent in the gel peak breaking force. 3D-printed HA/ND nanocomposite hydrogels with (Figure 5c) and without (Figure 5d) post-UV exposure were used to investigate the impact of pH on mechanical integrity. Both HA nanocomposite hydrogels containing ND-COOH or ND-OH showed higher peak forces at pH 8, compared to the same nanocomposite hydrogels prepared at pH 7. The difference in pH at the stage of nanocomposite hydrogel precursor resulted in the high peak force 0.905 N of HA/ND-OH (0.02 wt %) at pH 8, compared to 0.511 N of HA/ND-OH (0.02 wt %) at pH 7, revealing a 177 % boost in peak force. pH dependence became even more apparent when the composite amount was increased to 0.04 wt %, which showed the enhancement of the peak force with an increase in pH. The peak force 1.920 N of HA/ND-OH (0.04 wt %) at pH 8 showed 155 % amplified peak force, compared to 1.236 N of HA/ND-OH (0.04 wt %) at pH 7. The boosted mechanical properties of HA/ND-COOH showed the same pH dependent tendencies. Without post-UV exposure, the gel peak breaking force of the nanocomposite hydrogels at varied pH was

not critically different from any sample when compared to HA only hydrogels (Figure 5d). A change in the gel peak breaking force post-UV crosslinking confirmed that NDs within an HA matrix were spread out in a nanophase, thus concerting molecular environments that promoted interactions between the ND and HA. Hydrogels containing ND-OH showed the best performance at pH 8 and pH 7, compared to those with ND-COOH. The agglomerate stability of the ND varied depending on the pH and surface functionality in the aqueous dispersion [42]. State of ink precursors was a viscous dispersion of HA and ND before extrusion processing, and settled 3D firm hydrogels allowed for post-UV exposure, allowing for stable ND dispersion without confinement at local foci. Agglomerates of hydroxylated NDs are stable at both pH 7 and 8, while similar agglomerates of carboxylate ND are critically enhanced at pH 8 due to the deprotonation of the carboxyl group resulting in a hydrophilic surface. These intrinsic properties of NDs affect the distribution within the HA matrix, intermolecular electrostatic interaction, and hydrogel bonding through physical contact of gel network. Without chemical crosslinking, the physical network created by the addition of ND-COOH or ND-OH was able to achieve the mechanically stabilized 3D-printed hydrogel construction.

Conclusion

3D printing nanocomposite hydrogels composed of HA/ND achieved mechanically enforced compressive stress when compared with HA hydrogels. The addition of ND at a low weight ratio of 0.02 wt % increased the compressive force and gel breaking point. Surface functionalization of ND with carboxyl and hydroxyl group provided a tunable buffering environment and facilitated interaction with long HA chains at the molecular level, resulting in pH-dependent control of mechanical properties. The ND-OH nanophase, which was stable over a range of pH, improved mechanical stress compared to ND-COOH, indicating that the stability of inorganic compositing nanophases in an aqueous state is a critical parameter that affects mechanical properties of 3D-printed nanocomposite hydrogels. Herein, we have applied filament-based processing and layer-based deposition at the microscale, resulting in newly generated mechanical properties of nanocomposite hydrogels. Fine surface tuning of inorganic ND nanophases along with 3D-printed construction resulted in pH-dependent control over the mechanical properties of HA hydrogels, opening new potentials of metastatic soft and strong nanocomposite materials.

Declarations

Corresponding Author

*Correspondence to eakangek@cau.ac.kr (E.K.); shjeong@dongguk.edu (S.H.J.)

Author Contributions

The manuscript was written through contributions of all authors. All authors have given approval to the final version of the manuscript.

ACKNOWLEDGMENT

This research was supported by the Basic Science Research Program through the National Research Foundation of Korea (NRF) funded by the Ministry of Education (NRF-2018R1D1A1B07042982) and the National Research Foundation of Korea (NRF) grant funded by the Korea government (MSIT) (NRF-2018R1A5A2023127).

References

1. Alhnan MA, Okwuosa TC, Sadia M, Wan KW, Ahmed W, Arafat B. Emergence of 3D Printed Dosage Forms: Opportunities and Challenges. Pharm Res. 2016;33:1817-1832.
2. Gou M, Qu X, Zhu W, Xiang M, Yang J, Zhang K, Wei Y, Chen S. Bio-inspired detoxification using 3D-printed hydrogel nanocomposites. Nat Commun. 2014;5:1-9.
3. Jamroz W, Szafraniec J, Kurek M, Jachowicz R. 3D Printing in Pharmaceutical and Medical Applications - Recent Achievements and Challenges. Pharm Res. 2018;35:176.
4. Billiet T, Vandenhaute M, Schelfhout J, Van Vlierberghe S, Dubruel P. A review of trends and limitations in hydrogel-rapid prototyping for tissue engineering. Biomaterials. 2012;33:6020-6041.
5. Sowmya S, Mony U, Jayachandran P, Reshma S, Kumar RA, Arzate H, Nair SV, Jayakumar R. Tri-Layered Nanocomposite Hydrogel Scaffold for the Concurrent Regeneration of Cementum, Periodontal Ligament, and Alveolar Bone. Adv Healthc Mater. 2017;6:1601251.
6. Castro NJ, O'Brien J, Zhang LG. Integrating biologically inspired nanomaterials and table-top stereolithography for 3D printed biomimetic osteochondral scaffolds. Nanoscale. 2015;7:14010-14022.
7. Zhu W, Holmes B, Glazer RI, Zhang LG. 3D printed nanocomposite matrix for the study of breast cancer bone metastasis. Nanomedicine. 2016;12:69-79.
8. Xu C, Dai G, Hong Y. Recent advances in high-strength and elastic hydrogels for 3D printing in biomedical applications. Acta Biomater. 2019;95:50-59.
9. Yang B, Yuan W. Highly Stretchable, Adhesive, and Mechanical Zwitterionic Nanocomposite Hydrogel Biomimetic Skin. ACS Appl Mater Interfaces. 2019;11:40620-40628.
10. Chimene D, Kaunas R, Gaharwar AK. Hydrogel Bioink Reinforcement for Additive Manufacturing: A Focused Review of Emerging Strategies. Adv Mater. 2020;32:e1902026.
11. Hardin JO, Ober TJ, Valentine AD, Lewis JA. Microfluidic Printheads for Multimaterial 3D Printing of Viscoelastic Inks. Adv Mater. 2015;27:3279-3284.
12. Hsieh CT, Hsu SH. Double-Network Polyurethane-Gelatin Hydrogel with Tunable Modulus for High-Resolution 3D Bioprinting. ACS Appl Mater Interfaces. 2019;11:32746-32757.
13. Merino S, Martin C, Kostarelos K, Prato M, Vazquez E. Nanocomposite Hydrogels: 3D Polymer-Nanoparticle Synergies for On-Demand Drug Delivery. ACS Nano. 2015;9:4686-4697.
14. Hao N, Zhang X, Zhou Z, Hua R, Zhang Y, Liu Q, Qian J, Li H, Wang K. AgBr nanoparticles/3D nitrogen-doped graphene hydrogel for fabricating all-solid-state luminol-electrochemiluminescence Escherichia coli aptasensors. Biosens Bioelectron. 2017;97:377-383.

15. Skardal A, Zhang J, McCoard L, Oottamasathien S, Prestwich GD. Dynamically crosslinked gold nanoparticle - hyaluronan hydrogels. Adv Mater. 2010;22:4736-4740.
16. Liu J, Chen C, He C, Zhao J, Yang X, Wang H. Synthesis of graphene peroxide and its application in fabricating super extensible and highly resilient nanocomposite hydrogels. ACS Nano. 2012;6:8194-8202.
17. Olate-Moya F, Arens L, Wilhelm M, Mateos-Timoneda MA, Engel E, Palza H. Chondroinductive Alginate-Based Hydrogels Having Graphene Oxide for 3D Printed Scaffold Fabrication. ACS Appl Mater Interfaces. 2020;12:4343-4357.
18. Li J, Xie J, Gao L, Li CM. Au nanoparticles-3D graphene hydrogel nanocomposite to boost synergistically in situ detection sensitivity toward cell-released nitric oxide. ACS Appl Mater Interfaces. 2015;7:2726-2734.
19. Liu S, Bastola AK, Li L. A 3D Printable and Mechanically Robust Hydrogel Based on Alginate and Graphene Oxide. ACS Appl Mater Interfaces. 2017;9:41473-41481.
20. El-Fiqi A, Lee JH, Lee EJ, Kim HW. Collagen hydrogels incorporated with surface-aminated mesoporous nanobioactive glass: Improvement of physicochemical stability and mechanical properties is effective for hard tissue engineering. Acta Biomater. 2013;9:9508-9521.
21. Diloksumpan P, de Ruijter M, Castilho M, Gbureck U, Vermonden T, van Weeren PR, Malda J, Levato R. Combining multi-scale 3D printing technologies to engineer reinforced hydrogel-ceramic interfaces. Biofabrication. 2020;12:025014.
22. Kehr NS. Enantiomorphous Periodic Mesoporous Organosilica-Based Nanocomposite Hydrogel Scaffolds for Cell Adhesion and Cell Enrichment. Biomacromolecules. 2016;17:1117-1122.
23. Palaganas NB, Mangadlao JD, de Leon ACC, Palaganas JO, Pangilinan KD, Lee YJ, Advincula RC. 3D Printing of Photocurable Cellulose Nanocrystal Composite for Fabrication of Complex Architectures via Stereolithography. ACS Appl Mater Interfaces. 2017;9:34314-34324.
24. De France KJ, Chan KJ, Cranston ED, Hoare T. Enhanced Mechanical Properties in Cellulose Nanocrystal-Poly(oligoethylene glycol methacrylate) Injectable Nanocomposite Hydrogels through Control of Physical and Chemical Cross-Linking. Biomacromolecules. 2016;17:649-660.
25. Jin Y, Shen Y, Yin J, Qian J, Huang Y. Nanoclay-Based Self-Supporting Responsive Nanocomposite Hydrogels for Printing Applications. ACS Appl Mater Interfaces. 2018;10:10461-10470.
26. Zhai X, Ruan C, Ma Y, Cheng D, Wu M, Liu W, Zhao X, Pan H, Lu WW. 3D-Bioprinted Osteoblast-Laden Nanocomposite Hydrogel Constructs with Induced Microenvironments Promote Cell Viability, Differentiation, and Osteogenesis both In Vitro and In Vivo. Adv Sci (Weinh). 2018;5:1700550.
27. Deng Z, Hu T, Lei Q, He J, Ma PX, Guo B. Stimuli-Responsive Conductive Nanocomposite Hydrogels with High Stretchability, Self-Healing, Adhesiveness, and 3D Printability for Human Motion Sensing. ACS Appl Mater Interfaces. 2019;11:6796-6808.
28. Zhang Z, Xiao F, Guo Y, Wang S, Liu Y. One-pot self-assembled three-dimensional TiO2-graphene hydrogel with improved adsorption capacities and photocatalytic and electrochemical activities. ACS Appl Mater Interfaces. 2013;5:2227-2233.

29. Wang H, Morales RT, Cui X, Huang J, Qian W, Tong J, Chen W. A Photoresponsive Hyaluronan Hydrogel Nanocomposite for Dynamic Macrophage Immunomodulation. Adv Healthc Mater. 2019;8:e1801234.
30. Wu L, Chen G, Li Z. Layered Rare-Earth Hydroxide/Polyacrylamide Nanocomposite Hydrogels with Highly Tunable Photoluminescence. Small. 2017;13:1604070.
31. Ren Y, Feng J. Skin-Inspired Multifunctional Luminescent Hydrogel Containing Layered Rare-Earth Hydroxide with 3D Printability for Human Motion Sensing. ACS Appl Mater Interfaces. 2020;12:6797-6805.
32. Lee SS, Choi GE, Lee HJ, Kim Y, Choy JH, Jeong B. Layered Double Hydroxide and Polypeptide Thermogel Nanocomposite System for Chondrogenic Differentiation of Stem Cells. ACS Appl Mater Interfaces. 2017;9:42668-42675.
33. McCracken JM, Rauzan BM, Kjellman JCE, Kandel ME, Liu YH, Badea A, Miller LA, Rogers SA, Popescu G, Nuzzo RG. 3D-Printed Hydrogel Composites for Predictive Temporal (4D) Cellular Organizations and Patterned Biogenic Mineralization. Adv Healthc Mater. 2019;8:e1800788.
34. Burdick JA, Prestwich GD. Hyaluronic acid hydrogels for biomedical applications. Adv Mater. 2011;23:H41-H56.
35. Kiyotake EA, Douglas AW, Thomas EE, Nimmo SL, Detamore MS. Development and quantitative characterization of the precursor rheology of hyaluronic acid hydrogels for bioprinting. Acta Biomater. 2019;95:176-187.
36. Highley CB, Rodell CB, Burdick JA. Direct 3D Printing of Shear-Thinning Hydrogels into Self-Healing Hydrogels. Adv Mater. 2015;27:5075-5079.
37. Ouyang L, Highley CB, Rodell CB, Sun W, Burdick JA. 3D printing of shear-thinning hyaluronic acid hydrogels with secondary cross-linking. ACS Biomater Sci Eng. 2016;2:1743-1751.
38. Kim MC, Lee D, Jeong SH, Lee SY, Kang E. Nanodiamond-Gold Nanocomposites with the Peroxidase-Like Oxidative Catalytic Activity. ACS Appl Mater Interfaces. 2016;8:34317-34326.
39. Lee DK, Kee T, Liang Z, Hsiou D, Miya D, Wu B, Osawa E, Chow EK, Sung EC, Kang MK, Ho D. Clinical validation of a nanodiamond-embedded thermoplastic biomaterial. Proc Natl Acad Sci U S A. 2017;114:E9445-E9454.
40. Lim DG, Prim RE, Kim KH, Kang E, Park K, Jeong SH. Combinatorial nanodiamond in pharmaceutical and biomedical applications. Int J Pharm. 2016;514:41-51.
41. Mochalin VN, Shenderova O, Ho D, Gogotsi Y. The properties and applications of nanodiamonds. Nat Nanotechnol. 2011;7:11-23.
42. Lim DG, Jung JH, Ko HW, Kang E, Jeong SH. Paclitaxel-Nanodiamond Nanocomplexes Enhance Aqueous Dispersibility and Drug Retention in Cells. ACS Appl Mater Interfaces. 2016;8:23558-23567.
43. Lim DG, Rajasekaran N, Lee D, Kim NA, Jung HS, Hong S, Shin YK, Kang E, Jeong SH. Polyamidoamine-Decorated Nanodiamonds as a Hybrid Gene Delivery Vector and siRNA Structural Characterization at the Charged Interfaces. ACS Appl Mater Interfaces. 2017;9:31543-31556.

44. Shirani A, Hu Q, Su Y, Joy T, Zhu D, Berman D. Combined Tribological and Bactericidal Effect of Nanodiamonds as a Potential Lubricant for Artificial Joints. ACS Appl Mater Interfaces. 2019;11:43500-43508.
45. Hachet E, Van Den Berghe H, Bayma E, Block MR, Auzely-Velty R. Design of biomimetic cell-interactive substrates using hyaluronic acid hydrogels with tunable mechanical properties. Biomacromolecules. 2012;13:1818-1827.
46. Burdick JA, Chung C, Jia X, Randolph MA, Langer R. Controlled degradation and mechanical behavior of photopolymerized hyaluronic acid networks. Biomacromolecules. 2005;6:386-391.
47. Oliver WC, Pharr GM. An improved technique for determining hardness and elastic modulus using load and displacement sensing indentation experiments. J Mater Res. 1992;7:1564-1583.
48. Guvendiren M, Lu HD, Burdick JA. Shear-thinning hydrogels for biomedical applications. Soft matter. 2012;8:260-272.
49. Lee JM, Yeong WY. Design and Printing Strategies in 3D Bioprinting of Cell-Hydrogels: A Review. Adv Healthc Mater. 2016;5:2856-2865.
50. Petit T, Girard HA, Trouve A, Batonneau-Gener I, Bergonzo P, Arnault JC. Surface transfer doping can mediate both colloidal stability and self-assembly of nanodiamonds. Nanoscale. 2013;5:8958-8962.

Figures

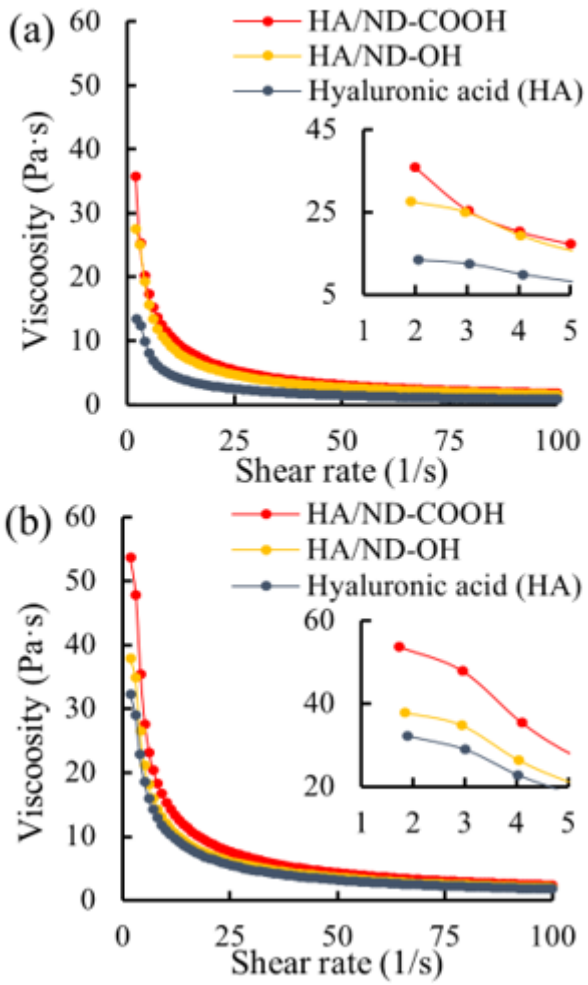

Figure 1

Viscosity vs. shear rate of HA nanocomposite hydrogel precursor composited with ND-OH or ND-COOH at (a) pH 7 and (b) pH 8.

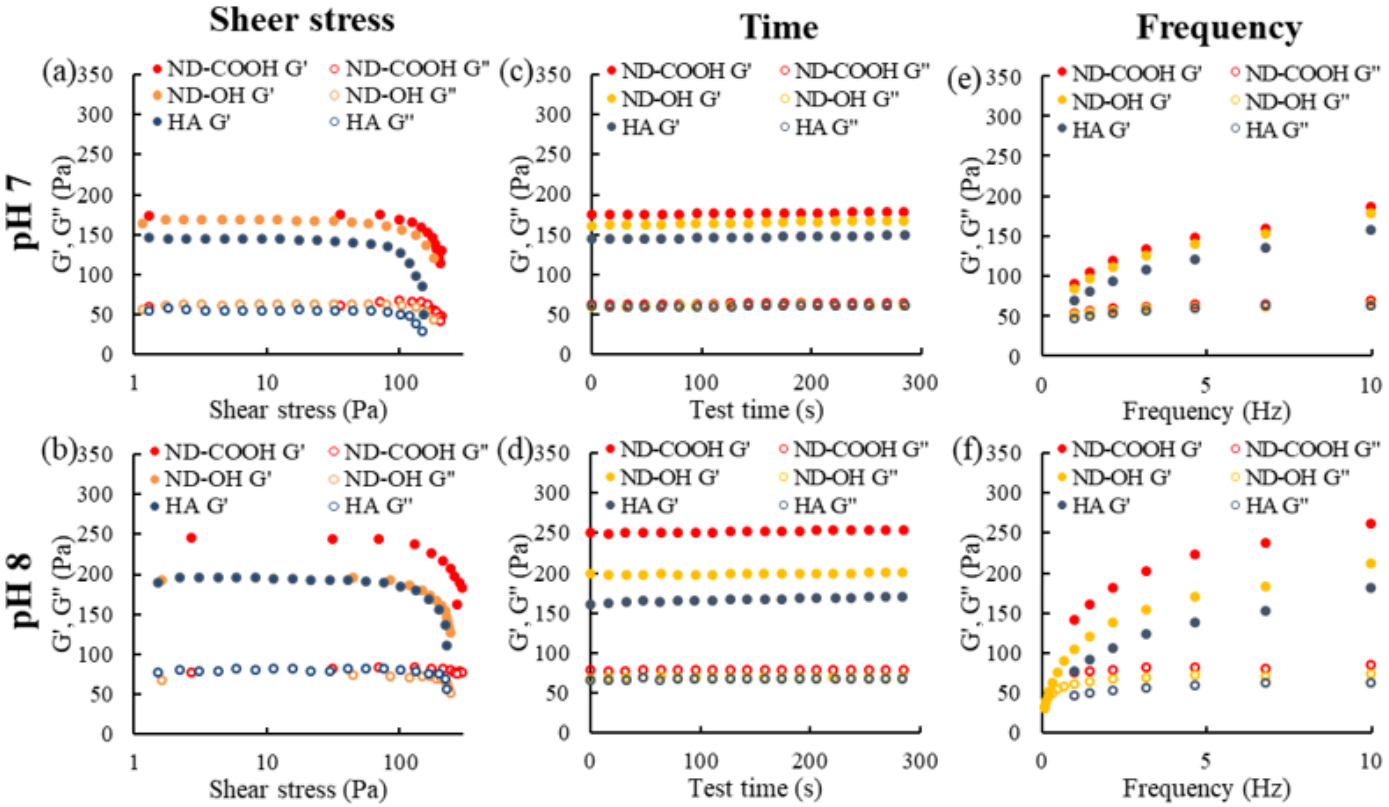

Figure 2

Rheological properties and relaxation behavior of nanocomposite hydrogel precursor of HA/ND. Storage modulus G' and Loss Modulus G" of HA and HA/ND hydrogel precursor mixed with 0.02 wt % as function of shear stress at (a) pH 7 and (b) pH 8. Storage modulus G' and Loss Modulus G" of HA and HA/ND as a function of time at (c) pH 7 and (d) pH 8. Storage modulus G' and Loss Modulus G" of HA and HA/ND as a function of frequency at (e) pH 7 and (f) pH 8.

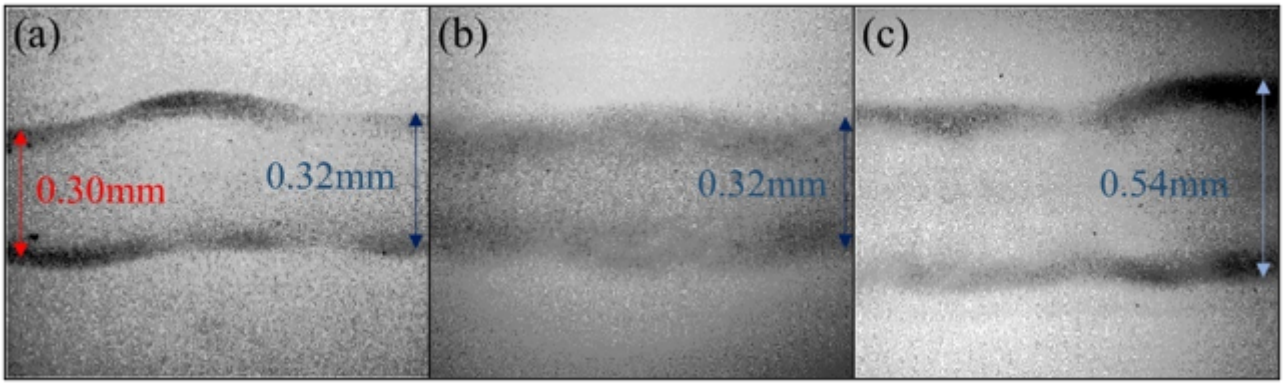

Figure 3

Filament sizes for the HA/ND-OH nanocomposite hydrogel precursor with varied needle size under the same printing parameter configurations (moving speed of 2 mm/s). Needle size: (a) 26 gauge, (b) 23 gauge, (c) 21 gauge.

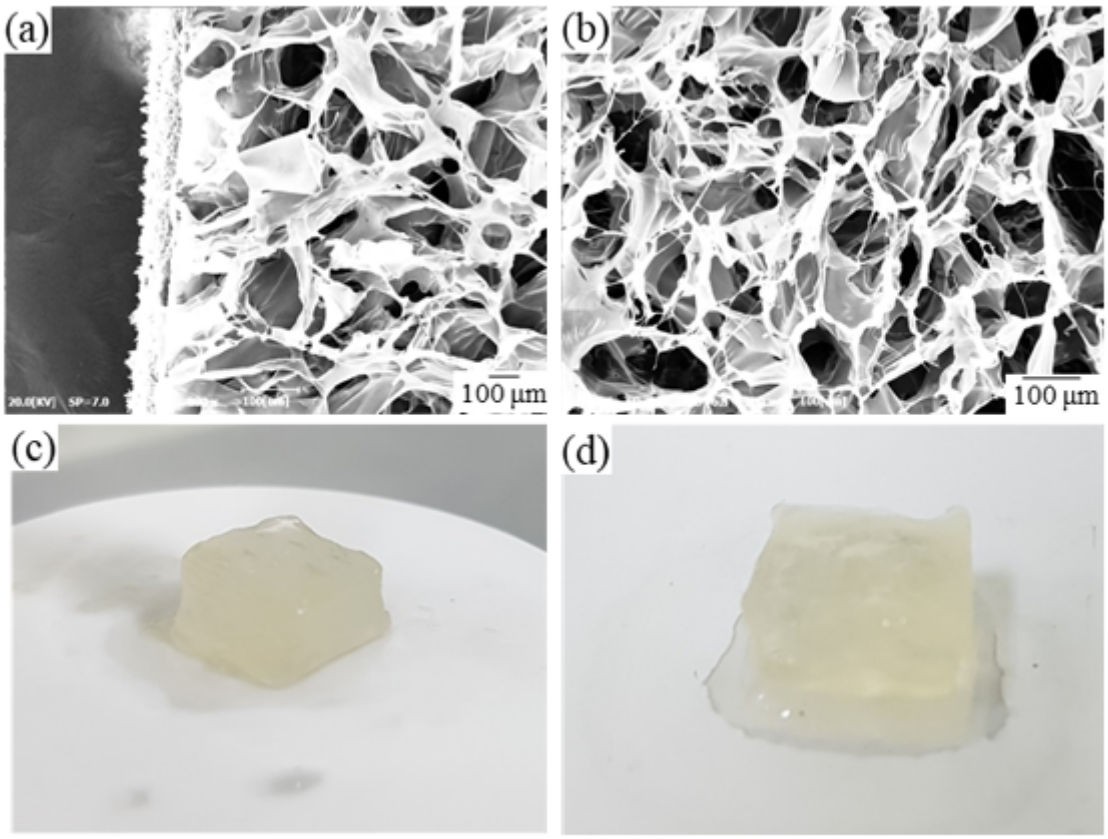

Figure 4

The porous network (a, b) and optical image (c, d) of 3D-printed crosslinked HA structure

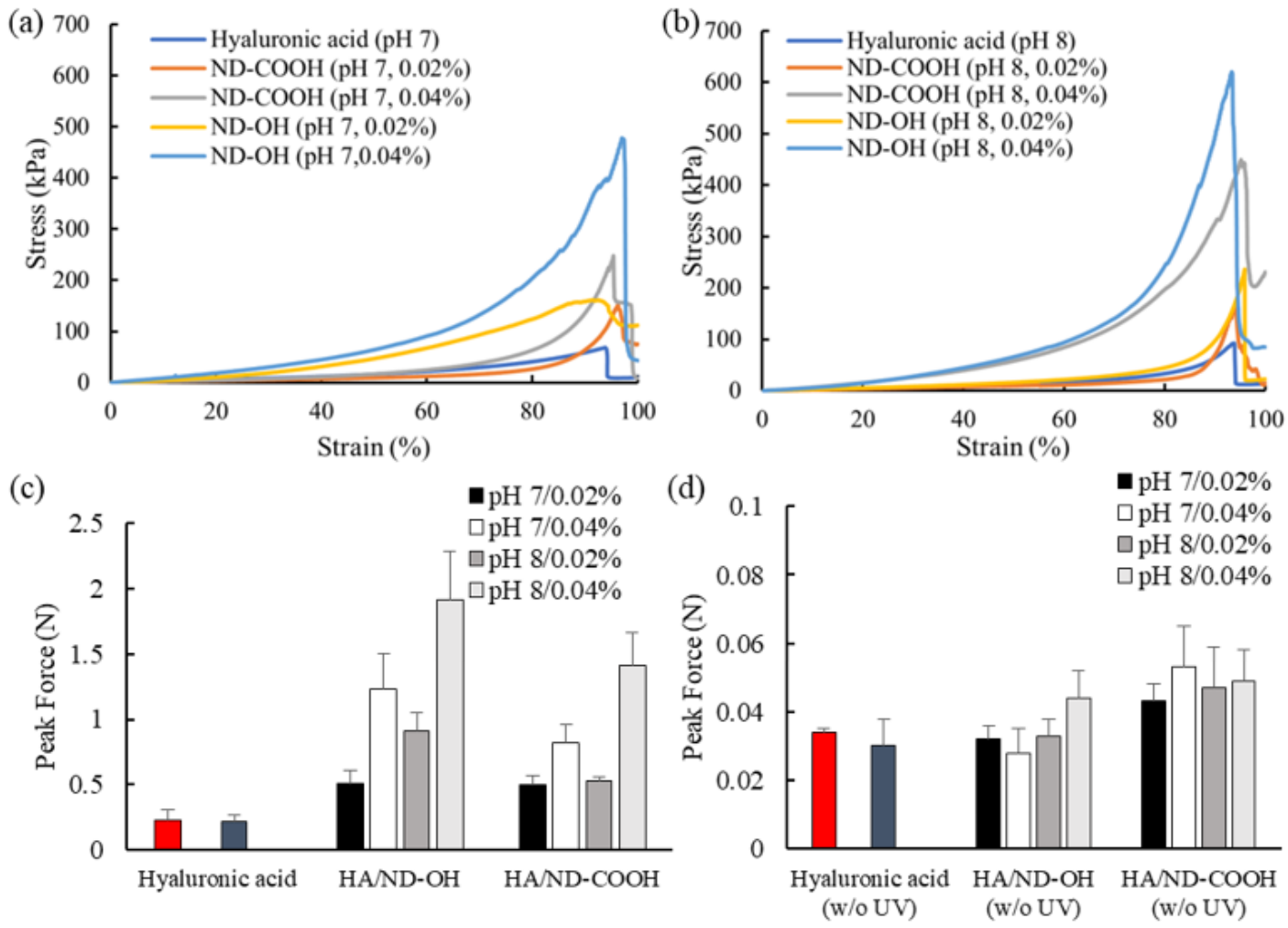

Figure 5

Compressive stress-strain curves of the HA nanocomposite hydrogels with ND-COOH or ND-OH at (a) pH 7 and (b) pH 8. (c) Gel breaking compressive peak force of the HA structures at pH 7 or 8 and surface functionalized NDs (HA without ND at pH 7 (red), pH 8 (blue)). (d) Compressive peak force of HA structure without post-UV exposure (HA without ND at pH 7 (red), pH 8 (dark gray)

Supplementary Files

This is a list of supplementary files associated with this preprint. Click to download.

- ExperimentalMethods.docx
- scheme.PNG
- graphicalabstract.PNG